REPUBLIC OF AZERBAIJAN

On the right of the manuscript

ABSTRACT

of the dissertation for the degree of Doctor of Philosophy

OBTAINING MATERIALS WITH TOPOLOGICAL INSULATOR PROPERTIES BASED ON LEAD-BISMUTH TELLURIDES AND MODELING THEIR PHASE DIAGRAMS

Speciality: 2307.01 – Physical Chemistry

Field of science: Chemistry

Applicant: **Aytan Ismat Aghazade**

Baku – 2025

The work was performed at the laboratory "Thermodynamics of functional inorganic compounds" at the Institute of Catalysis and Inorganic Chemistry named after academician M.Nagiyev of the Ministry of Science and Education.

Scientific supervisor: Doctor of Chemical Science, Professor
Asif Nasib Mammadov

Scientific consultant: Corresponding member of ANAS,
Doctor of Chemical Science, Professor
Mahammad Baba Babanly

Official opponents: Corresponding member of ANAS,
Doctor of Chemical Science, Professor
Tofig Abbasali Aliyev

Doctor of Chemical Science, Professor
Yasin İsa Jafarov

Doctor of Philosophy Chemistry
Ganira Babashirin Balakishiyeva

Dissertation Council ED 2.16 of Supreme Attestation Commission under the President of the Republic of Azerbaijan operating at Baku State University

Chairman of the Dissertation Council:
Doctor of Chemical Science, Professor
Ibrahim Garib Mammadov

Scientific Secretary of the Dissertation Council:
Doctor of Chemical Science,
Associate Professor
Farid Nadir Naghiyev

Chairman of the Scientific Seminar:
Doctor of Chemical Science,
Associate Professor
Dunya Mahammad Babanly

BAKI DÖVLƏT UNİVERSİTETİ
SCIENTIFIC SECRETARY
"07" 04 2025

GENERAL CHARACTERISTICS OF THE WORK

Relevance of the topic and the degree of development. Similar to many other fields of science, modern chemistry has undergone rapid development. This is attributed to the application of information technologies to science, the invention of highly sensitive measuring devices, and the discovery of materials exhibiting qualitatively novel functional properties. Research into the revelation of such materials, developing synthesis methods, and optimizing their properties represents one of the main prospective directions in modern chemistry. Achieving and optimizing these processes necessitate mathematical modeling, including 3D modeling of phase diagrams, which is crucial. Consequently, the search for new complex inorganic functional materials, their synthesis, and the modeling of phase diagrams in relevant systems are among the pressing issues of contemporary materials science.

The discovery of a new quantum state of matter – the topological insulator[1] (TI) – in the early 21st century greatly accelerated advancements in electronic technologies. TI materials possess unique quantum properties: they are dielectric in the bulk but exhibit high electrical conductivity on their surfaces. Since TIs retain topological properties at high temperatures, they are of significant interest for applications in computer technologies and microelectronics. Additionally, the spin character of topological insulators promises bright prospects in the field of spintronics for storing and transmitting information[2].

Analysis of the literature indicates that the ternary layered compounds ($A^{IV}B^{V}_2Te_4$, $A^{IV}B^{V}_4Te_7$, $A^{IV}B^{V}_6Te_{10}$, $A^{IV}B^{V}_8Te_{13}$) in the $A^{IV}Te$-$B^{V}_2Te_3$ (A^{IV}- Ge, Sn, Pb; B^{V}- Sb, Bi) systems are widely studied as topological insulators. Studies on the phase equilibria and thermodynamic properties of these systems facilitate the search for new compounds, solid solutions, and intermediate phases, significantly expanding the scope of investigated substances[3].

---

[1] Moore, J.E. The Birth of Topological Insulators // Nature, - 2010. 464, - p.194- 198.

[2] Hasan, M.Z. Topological Insulators // Review of Modern Physics, - 2010. 82(4), - p. 3045-3067.

[3] Babanly, M.B. Phase diagrams in materials science of topological insulators based on metal chalcogenides / M.B. Babanly, E.V. Chulkov, Z.S. Aliev [et al.] // - Moscow: Russian Journal of Inorganic Chemistry, - 2017. 62 (13), - p. 1703–1729

In this regard, quasi-ternary systems composed of $A^{IV}Te$ and $B^{V}_2Te_3$ compounds are highly promising for obtaining new materials with topological insulator properties. Wide solid solution regions are expected to form in the boundary quasi-binary sections of such systems, based on the layered structures of ternary compounds, enabling optimization of functional properties through compositional variations. However, literature data show that the phase equilibria in such systems have scarcely been studied.

On the other hand, the search, synthesis, and design of new phases with TI properties require advanced approaches, such as the principle of fuzzy systems, for obtaining alloys close to equilibrium and studying phase equilibria. In recent years, the optimization of phase equilibrium coordinates has been carried out using the "Multipurpose Genetic Algorithm" (MGA) to better align thermodynamic models with limited experimental data[4].

Object and subject of research. Considering the above, the research objects in this dissertation are the PbTe-Bi_2Te_3-Sb_2Te_3 and SnTe-PbTe-Bi_2Te_3 systems. The subject of the research is the determination of phase equilibrium landscapes and the mathematical modeling of phase diagrams in these systems.

Goal and objectives of the research. The goal of the dissertation is to determine the nature of physicochemical interactions in the PbTe-Bi_2Te_3-Sb_2Te_3 and SnTe-PbTe-Bi_2Te_3systems, model their T-x-y phase diagrams, and conduct thermodynamic analysis.

To achieve this goal, the following **specific tasks** were set and solved:

- Synthesizing and physicochemically studying samples as close as possible to equilibrium states in the PbTe-Bi_2Te_3-Sb_2Te_3 and SnTe-PbTe-Bi_2Te_3 systems;
- Determining the phase equilibrium landscapes in these systems, constructing projections of liquidus surfaces, and various polythermal and isothermal sections of phase diagrams, as well as identifying the

[4] Babanly, N.B. Determination and modeling of the liquidus surface, vapor pressure and immiscibility boundaries in the Cu–Pb–S system / N.B.Babanly, M.V.Bulanova, A.N.Mustafaeva // Azerbaijan Chemical Journal, – 2021. № 4. – p. 35–42.

types and coordinates of non- and monovariant equilibria;

- Analytical 3D modeling and thermodynamic analysis of the phase diagrams for the $PbTe\text{-}Bi_2Te_3\text{-}Sb_2Te_3$ and $SnTe\text{-}PbTe\text{-}Bi_2Te_3$ systems.

Research methods. Experimental studies within the dissertation were conducted using traditional methods of physicochemical analysis, including differential thermal analysis (DTA), differential scanning calorimetry (DSC), X-ray diffraction analysis (XRD), scanning electron microscopy (SEM), and microstructural analysis. DTA was performed using a multichannel device based on the "TC-08 Thermocouple Data Logger" electronic recorder, as well as "NETZSCH 404 F1 Pegasus system" and LINSEIS HDSC PT1600 devices. The powder diffraction patterns were obtained using a D2 Phaser device from Bruker, Germany, and analyzed using the software provided with this type of diffractometer. Microstructural analysis was carried out using a Tescan Vega 3 SBH scanning electron microscope equipped with a Thermo Scientific UltrDry Compact EDS detector.

The fundamental principles of physicochemical analysis and phase equilibrium thermodynamics, as well as the principles of fuzzy logic, were utilized in the research. OriginLab software was used to obtain 3D model visualizations.

Main provisions presented for defense.

1. Phase diagrams of the $PbTe\text{-}Bi_2Te_3\text{-}Sb_2Te_3$ and $SnTe\text{-}PbTe\text{-}Bi_2Te_3$ systems, including several polythermal and isothermal sections and projections of liquidus surfaces;
2. Initial crystallization regions of phases identified in the phase diagrams of the studied systems, along with the types and coordinates of non- and monovariant equilibria;
3. Thermal and crystallographic parameters of cation-substituted solid solutions determined in both systems;
4. Analytical expressions and 3D models of initial crystallization regions for various phases in the $PbTe\text{-}Bi_2Te_3\text{-}Sb_2Te_3$ and $SnTe\text{-}PbTe\text{-}Bi_2Te_3$ systems.

Scientific novelty of the research. The following new scientific results were obtained in the dissertation:

- New, reliable phase equilibrium landscapes for the $PbTe$-Bi_2Te_3-Sb_2Te_3 and $SnTe$-$PbTe$-Bi_2Te_3 systems have been obtained. Projections of the liquidus surfaces and several polythermal and isothermal sections of phase diagrams were constructed for both systems. It was demonstrated that both systems are quasi-ternary planes of respective four-component systems;
- It was determined that the $PbTe$-Bi_2Te_3-Sb_2Te_3 system contains extensive solid solution regions based on the $PbBi_2Te_4$, $PbBi_4Te_7$, and $PbBi_6Te_{10}$ compounds, while in the $SnTe$-$PbTe$-Bi_2Te_3 system, continuous solid solution series exist between these ternary compounds and their tin analogs. Furthermore, extensive homogeneity regions involving Sn→Pb substitutions were identified in the $Sn_2Bi_2Te_5$ and $Sn_3Bi_2Te_6$ compounds within the $SnTe$-$PbTe$-Bi_2Te_3 system;
- Initial crystallization of six phases from the liquid phase was identified in both quasi-ternary systems, and the monovariant and nonvariant equilibria delimiting the liquidus surfaces of these phases were determined. The coordinates of the corresponding curves and points were specified;
- Samples of solid solutions of varying compositions, based on ternary compounds, were obtained in pure form in both systems. X-ray powder diffraction established their crystallization in layered structures resembling tetradymite, and lattice parameters were calculated;
- Using thermodynamic criteria for phase equilibria and principles of fuzzy logic, the liquidus and solidus surfaces (curves) of binary and ternary compounds were refined for the $PbTe$-Bi_2Te_3-Sb_2Te_3 and $SnTe$-$PbTe$-Bi_2Te_3 systems;
- Analytical expressions of the liquidus surfaces of all phases in the T-x-y diagrams of both quasi-ternary systems were obtained, and 3D models were developed and visualized.

Theoretical and practical significance of the research. The phase diagrams and multi-3D models constructed based on experimental studies contribute to the chemistry and materials science of layered chalcogenides and functional materials derived from them. Newly identified variable-composition phases in the investigated systems have potential

applications as topological insulators and thermoelectric materials.

The practical significance of the research lies in the applicability of the constructed phase diagrams, crystallographic parameters of various solid solution phases, and thermodynamic properties of phases as fundamental physicochemical parameters for inclusion in relevant electronic information systems and data books. According to data from the "Google Scholar Citations" information system, 4 articles by the author on the dissertation topic published in international scientific journals have been cited 9 times.

Approbation and application. A total of 15 scientific works have been published on the dissertation topic. Of these, 6 articles were published in journals indexed in international databases such as Web of Science and Scopus. 9 scientific papers were presented at international conferences as conference materials and abstracts.

The main results of the dissertation were presented and discussed at the following scientific conferences: 9th Rostocker International Conference: "Thermophysical Properties for Technical Thermodynamics", Rostock, Germany (15 October, 2020); 10th Rostocker International Conference: "Thermophysical Properties for Technical Thermodynamics", Rostock, Germany (09-10 September, 2021); International scientific conference on "Current problems of natural and economic sciences," Ganja, Azerbaijan (06-07 May, 2021); "1st International congress on natural sciences", (ICNAS)- Erzurum, Turkey (10-12 September, 2021); XI International Scientific Conference "Kinetics and Mechanism of Crystallization. Crystallization as a Form of Self-Organization of Matter," Ivanovo, Russia (20-24 September, 2021); "Physicochemical Processes in Condensed Media and at Interphase Boundaries," Voronezh, Russia (04-07 October, 2021); International scientific conference on "Current problems of natural and economic sciences," Ganja, Azerbaijan (06-07 May, 2022); XXIII International Conference on Chemical Thermodynamics, Kazan, Russia (22-27 August, 2022) ; International scientific conference on "Current problems of natural and economic sciences," Ganja, Azerbaijan (05-06 May, 2023).

Name of the organization where the dissertation is performed. The dissertation was performed at the "Thermodynamics of functional

inorganic compounds" laboratory of the Institute of Catalysis and Inorganic Chemistry named after academician M. Naghiyev of the Ministry of Science and Education.

Personal contribution of the author. The principal role in conducting the dissertation research and solving the assigned tasks belonged to the applicant. The author directly participated in carrying out experimental studies, summarizing and finalizing the obtained results, and preparing the materials for publication. The author made a decisive contribution to the co-authored scientific works.

The total volume of the dissertation with a sign, indicating the volume of the structural units of the dissertation separately. The dissertation (170078 characters) consists of an introduction (11051 characters), four chapters (first chapter - 52270 characters, second chapter - 36303 characters, third chapter - 32173 characters, fourth chapter - 34861 characters), main conclusions (3420 characters) and a list of used scientific literature. The dissertation includes 55 figures and 6 tables.

The introduction (11051 characters) provides information about the relevance of the topic, degree of development, object, subject, objectives, research methods, main provisions for defense, scientific novelty, theoretical and practical significance, approval, and application of the work, as well as the author's personal contribution to the research.

Chapter 1 (52270 characters): mainly provides literature data from the last 10 years and their analysis.

Chapter 2 (36303 characters): describes the synthesis and physicochemical analysis methods used in the dissertation.

Chapter 3 (32173 characters): presents T-x-y diagrams, isothermal and polythermal sections, initial crystallization fields of phases, as well as types and coordinates of monovariant and nonvariant equilibria for the $PbTe$-Bi_2Te_3-Sb_2Te_3 and $SnTe$-$PbTe$-Bi_2Te_3 systems.

Chapter 4 (34861 characters): describes results related to the analytical 3D modeling and thermodynamic analysis of phase diagrams for these quasi-ternary systems.

Finally, the *Conclusions* (3420 characters) section summarizes the research conducted and the results obtained.

MAIN CONTENT OF THE WORK

The introduction substantiates the relevance of the dissertation topic and presents its purpose, scientific novelty, practical significance, and main provisions for defense.

Chapter 1: Literature Review (52270 characters) This chapter provides an extensive review of recent literature, primarily from the last decade, analyzing the phase equilibria, thermodynamic, crystallographic, and physical-chemical properties of the binary and boundary quasi-binary systems comprising the initial components of the PbTe-Bi_2Te_3-Sb_2Te_3 and SnTe-PbTe-Bi_2Te_3 systems.

Additionally, modern studies on the thermoelectric and topological insulator properties of tetradymite-like layered tellurides are reviewed. The justification for selecting the dissertation topic is also presented.

Chapter 2: Experimental methods and materials (36303 characters) This chapter describes the synthesis methods for metal chalcogenides and the techniques used to study phase equilibria, such as DTA, XRD, SEM, and microstructural analysis. It also discusses approaches for calculating and modeling phase diagrams.

Initially, binary compounds PbTe, SnTe, Sb_2Te_3, and Bi_2Te_3 were synthesized as building blocks for the ternary systems. The synthesis was carried out by co-melting high-purity elemental components in quartz ampoules in a single-zone furnace at a temperature about 50°C above the melting point, followed by gradual cooling to room temperature. The synthesized samples were identified using DTA and XRD methods.

The alloys of both studied systems were then synthesized using the pre-prepared binary compounds. Samples of approximately 1 gram were prepared with 5–10 mol% composition intervals along different sections of the ternary systems. The stoichiometric mixtures were sealed in evacuated quartz ampoules, melted, and treated thermally for homogenization.

Structural insights of layered compounds: The ternary compounds in the studied systems possess tetradymite-like layered structures. Within these structures, strong chemical bonds exist between atoms within layers, while weak van der Waals forces are present between layers. This configuration facilitates significant diffusion within layers at high temperatures, ensuring intralayer equilibrium. However, the weak interlayer

bonds hinder diffusion across layers, complicating the attainment of full equilibrium in the material.

Due to these structural peculiarities, the traditional method of comelting, cooling, and thermal treatment is insufficient for synthesizing equilibrium phases. To overcome this, the molten alloys were held at a temperature 50–100 K above the liquidus for 3–4 hours and then quenched in cold water. This rapid cooling inhibits crystal growth, resulting in ultrafine micro- and nanocrystals, which were subsequently subjected to prolonged thermal treatment at temperatures 30–50 K below the solidus for 30–90 days to reach equilibrium.

Chapter 3: Phase equilibria in PbTe-Bi_2Te_3-Sb_2Te_3 and SnTe-PbTe-Bi_2Te_3 systems (32173 characters). This chapter presents the results of phase equilibrium studies.

The results of the study of these systems are reflected in the works [1-3, 6-10, 13].

Chapter 4: The results of analytical 3D modeling and thermo dynamic analysis of phase diagrams of PbTe-Bi_2Te_3-Sb_2Te_3 and SnTe-PbTe-Bi_2Te_3 quasi-ternary systems are given (34861 characters).

The results of the study of these systems are reflected in [4, 5, 11, 12, 14, 15].

Phase equilibria in system PbTe-Bi_2Te_3-Sb_2Te_3.

Analysis of the synthesized and thermally treated samples using methods described in Chapter 2, combined with literature data on boundary quasi-binary sections, enabled the construction of the general phase equilibrium landscape for the PbTe-Bi_2Te_3-Sb_2Te_3 system.

The solid phase equilibria. Figure1 shows a diagram of solid-state equilibria at 500 K for the PbTe-Bi_2Te_3-Sb_2Te_3 system. A phase diagram at 500 K revealed broad solid solution regions based on $PbBi_2Te_4$, $PbBi_4Te_7$, and $PbBi_6Te_{10}$ compounds, with Bi→Sb substitution. The continuous solid solution region observed in the Bi_2Te_3-Sb_2Te_3 boundary system penetrates the compositional triangle, forming a homogeneity band approximately 2–8 mol% wide. The phase equilibria analysis identified multiple biphasic regions (α+γ, γ+δ, δ+ε, β+ε, β+δ, β+γ, α+β), and three three-phase regions (α+β+γ, β+γ+δ, β+δ+ε). The results indicate that the formation of heterogeneous phases predominantly involves solid solution regions rather than stoichiometric phases.

The diffraction patterns of samples containing 20, 30, 40, 50, 60, and 80 mol% $PbBi_2Te_4$, subjected to thermal treatment along the $PbBi_2Te_4$ – "$PbSb_2Te_4$" section, were recorded. Figure 2(a) shows the diffraction pattern of the $PbBi_2Te_4$ compound, while Figures 2(b) and 2(c) display the diffraction patterns of alloys containing 80 and 50 mol% $PbBi_2Te_4$, respectively. As seen, the alloys with 50 and 80 mol% $PbBi_2Te_4$ exhibit diffraction patterns qualitatively identical to that of the $PbBi_2Te_4$ compound. However, the diffraction lines are slightly shifted relative to $PbBi_2Te_4$, indicating changes in lattice parameters due to the formation of solid solutions.

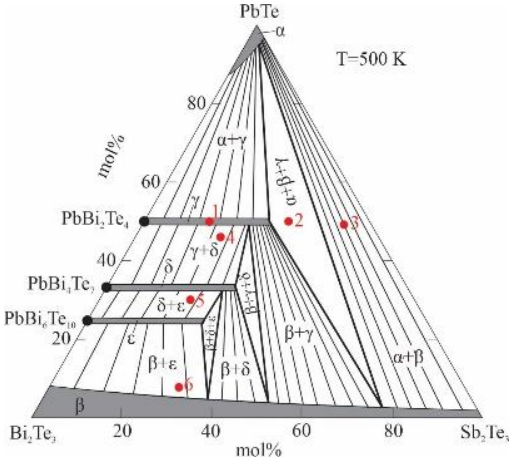

Figure 1. Solid-state equilibria diagram of the $PbTe$-Bi_2Te_3-Sb_2Te_3 system at 500 K

The diffractograms given in Figure 2 show these compositions, respectively: a) $PbBi_2Te_4$ birləşməsi, b) 80 mol% $PbBi_2Te_4$, c) 50 mol% $PbBi_2Te_4$, d) 40 mol% $PbBi_2Te_4$, e) 20 mol% $PbBi_2Te_4$.

The diffraction patterns of samples containing 20 and 40 mol% $PbBi_2Te_4$ (Figures 2(e) and 2(d)) reveal their heterogeneous nature. Analyses showed that these samples are two-phase and three-phase systems, respectively. The reflection angles of the α-phase coincide with the diffraction lines of PbTe, while the diffraction lines of the β-phase, based on Sb_2Te_3, are slightly shifted toward smaller angles compared to pure Sb_2Te_3. This is attributed to the formation of continuous solid solutions in the Bi_2Te_3–Sb_2Te_3 system.

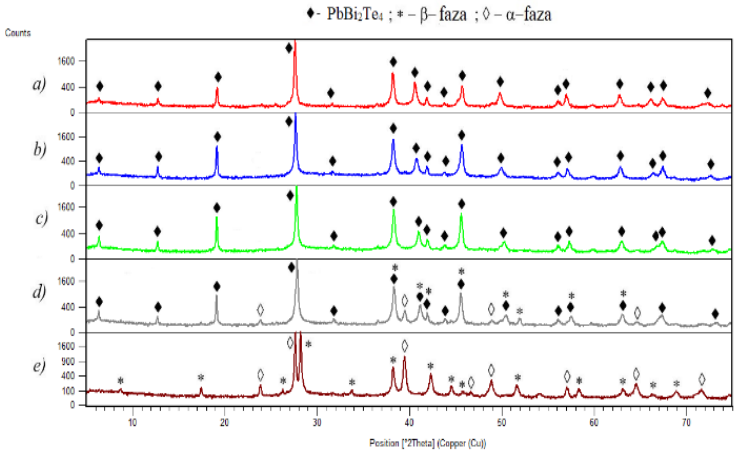

Figure 2. PXRD results on section $PbBi_2Te_4$-"$PbSb_2Te_4$"

Figure 3 presents SEM results for some samples along the $PbBi_2Te_4$ – "$PbSb_2Te_4$" section (1, 2, and 3 in Figure 1), confirming phase equilibria in Figure 1.

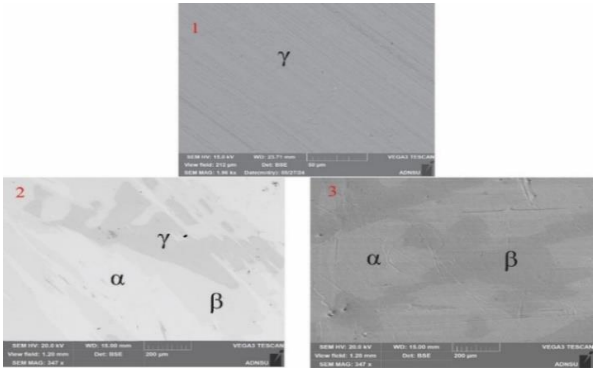

Figure 3. SEM images of samples 1, 2 and 3 as it shown in Figure 1

The dissertation also presents the powder XRD results of certain alloys along the $PbBi_4Te_7$-"$PbSb_4Te_7$" and $PbBi_6Te_{10}$-"$PbSb_6Te_{10}$" sections, as well as the crystallographic indices and isopleth sections of solid solutions formed in these sections.

The liquidus surface. For all studied samples, combining the DTA, XRD, and SEM results with literature data on phase equilibria

and intermediate phase properties in boundary quasi-binary systems, the projection of the liquidus surfaces of the $PbTe$-Bi_2Te_3-Sb_2Te_3 system was constructed (Figure 4).

The liquidus surface consists of six primary crystallization surfaces. A large portion (>90%) of the concentration triangle is occupied by the liquidus surfaces of the α- and β-phases (regions 1 and 2). The crystallization areas of the γ-, δ-, and ε-phases (regions 3–5), as well as the η-phase based on the $Pb_2Sb_6Te_{11}$ compound (region 6), are narrow bands located outside the compositions of these phases. The mentioned liquidus surfaces are bounded by several nonvariant equilibrium points and monovariant equilibrium curves. The types and temperatures of these equilibria are provided in Table 1.

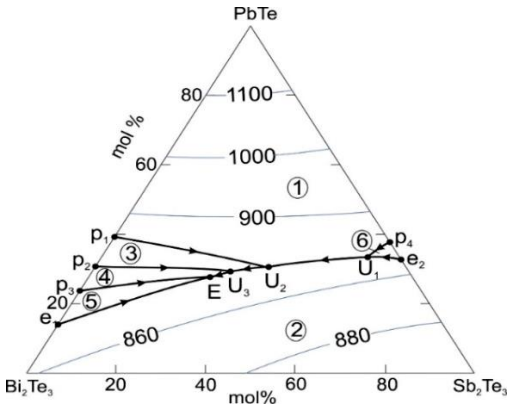

Figure 4. Projection of the liquidus surface of the $PbTe$-Bi_2Te_3-Sb_2Te_3 system. Primary crystallization areas: (1) α- phase; (2) β- phase; (3) γ- phase; (4) δ- phase; (5) ε- phase; (6) η- phase

The data in Figure 4 and Table 1 indicate that the interactions of monovariant equilibrium curves result in three transitional equilibria (U_1, U_2, U_3) and one ternary eutectic (E) in the system. The convergence of peritectic and eutectic curves originating from points P_4 and e_2 and the formation of the U1 equilibrium confirm the results of studies indicating that the $Pb_2Sb_6Te_{11}$ compound exists in the $PbTe$-Sb_2Te_3 system over a very narrow temperature range and decomposes through a solid-phase reaction.

Table 1

Nonvariant and monovariant equilibria in the PbTe-Bi_2Te_3-Sb_2Te_3 system

Point or curve in Figure 5	Equilibria	Thermal effects, K
P_1	$L+\alpha \leftrightarrow \gamma$ ($PbBi_2Te_4$)	864
P_2	$L+\gamma \leftrightarrow \delta$ ($PbBi_4Te_7$)	856
P_3	$L+\delta \leftrightarrow \varepsilon$ ($PbBi_6Te_{10}$)	851
P_4	$L+\alpha \leftrightarrow \eta$ ($Pb_2Sb_6Te_{11}$)	860
e_1	$L \leftrightarrow \varepsilon + \beta$	847
e_2	$L \leftrightarrow \eta + \beta$	856
U_1	$L + \eta \leftrightarrow \alpha + \beta$	854
U_2	$L + \alpha \leftrightarrow \beta + \gamma$	850
U_3	$L + \gamma \leftrightarrow \beta + \delta$	846
E	$L \leftrightarrow \beta + \delta + \varepsilon$	842
P_4U_1	$L + \alpha \leftrightarrow \eta$	860-854
e_2U_1	$L \leftrightarrow \eta + \beta$	856-854
U_1U_2	$L \leftrightarrow \alpha + \beta$	854-850
P_1U_2	$L + \alpha \leftrightarrow \gamma$	864-850
U_2U_3	$L \leftrightarrow \beta + \gamma$	850-846
P_2U_3	$L + \gamma \leftrightarrow \delta$	856-846
U_3E	$L \leftrightarrow \beta + \delta$	846-842
P_3E	$L + \delta \leftrightarrow \varepsilon$	851-842
e_1E	$L \leftrightarrow \beta + \varepsilon$	847-842

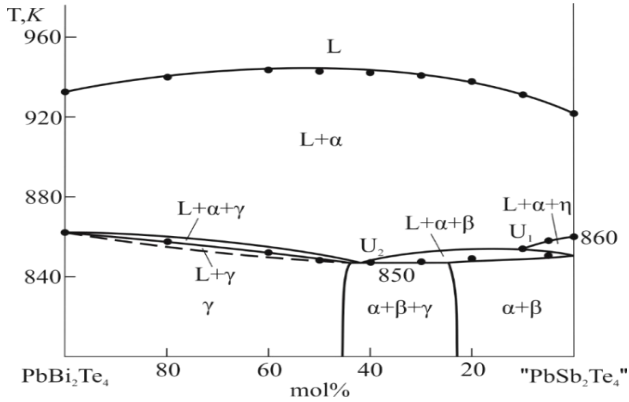

Figure 5. Isopleth section $PbBi_2Te_4$-"$PbSb_2Te_4$" of the phase diagram Phase equilibria in system SnTe-PbTe-Bi_2Te_3.

Some isopleth sections of the phase diagram. Figure 5 shows the isopleth section of $PbBi_2Te_4$-"$PbSb_2Te_4$". Since this section is entirely located within the primary crystallization field of the α-phase based on PbTe, this phase initially crystallizes from the melt, forming the L+α region. Crystallization then progresses (from right to left in Figure 5) through P_4U_1, U_1U_2, and P_1U_2 monovariant reactions and U_1 and U_2 transitional reactions. Crystallization ends as follows: in the 0–25 mol% $PbBi_2Te_4$ concentration range via the L↔α+β (U_1U_2) monovariant reaction, yielding the α+β mixture, and in the 45–100 mol% $PbBi_2Te_4$ range via the L+α↔γ (P_1U_2) reaction, producing the homogeneous γ-phase. In the intermediate region, crystallization concludes with the L+α↔β+γ (U_2) transitional reaction, resulting in the three-phase α+β+γ state.

The solid phase equilibria. To obtain a general view of the solid-phase equilibria diagram in the SnTe-PbTe-Bi_2Te_3 system synthesized and thermally treated samples were studied using the methods described in Chapter 2. These results, along with boundary quasibinary section literature data, were analyzed together.

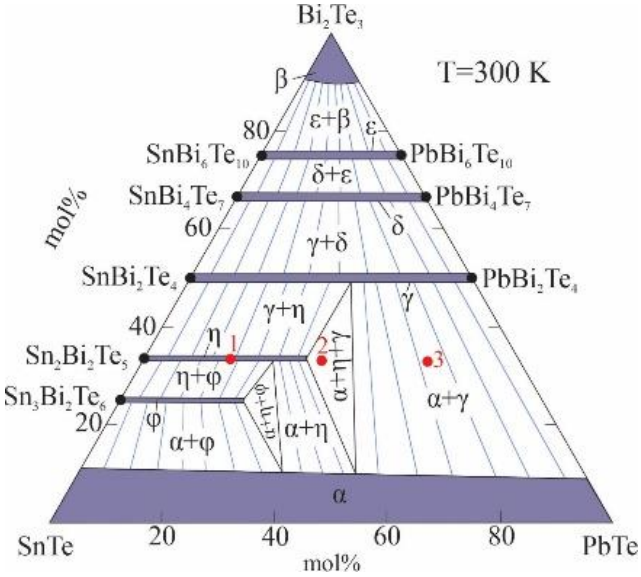

Figure 6. Solid-state equilibria diagram of the SnTe-PbTe-Bi_2Te_3 system

As shown in Figure 6, there are seven single-phase fields in the SnTe-PbTe-Bi_2Te_3 system: the β-phase based on Bi_2Te_3, the α-phase based on PbTe, continuous solid solution fields (γ, δ, ε phases) formed along the $SnBi_2Te_4$-$PbBi_2Te_4$, $SnBi_4Te_7$-$PbBi_4Te_7$, and $SnBi_6Te_{10}$-$PbBi_6Te_{10}$ sections, respectively. Single-phase fields η and φ based on the compounds $Sn_2Bi_2Te_5$ and $Sn_3Bi_2Te_6$. In addition, eight biphasic fields are formed: ε+β, δ+ε, γ+δ, γ+η, η+φ, α+φ, α+η, and α+γ. Furthermore, the system contains two triphasic regions: α+η+φ and α+η+γ.

The diffractograms in Figure 7 show these compositions: a) $Sn_2Bi_2Te_5$ birləşməsi; b) 80 mol% $Sn_2Bi_2Te_5$; c) 60 mol% $Sn_2Bi_2Te_5$; d) 50 mol% $Sn_2Bi_2Te_5$; e) 40 mol% $Sn_2Bi_2Te_5$; f) 20 mol% $Sn_2Bi_2Te_5$.

Figure 7 presents the powder XRD results of annealed samples for the $SnBi_2Te_4$-$PbBi_2Te_4$ (a), $SnBi_4Te_7$-$PbBi_4Te_7$ (b), and $SnBi_6Te_{10}$-$PbBi_6Te_{10}$ (c) sections. A comparison of the diffractograms shows that the diffraction patterns of all intermediate compositions are qualitatively similar to the initial ternary compounds and have a hexagonal structure of the tetradymite type with an *R-3m* space group.

Figure 8 shows the diffraction patterns of crushed samples with 20, 40, 50, 60, and 80 mol% $Sn_2Bi_2Te_5$ compositions from the $Sn_2Bi_2Te_5$-$Pb_2Bi_2Te_5$ section. The diffraction patterns of the 80, 60, and 50 mol% $Sn_2Bi_2Te_5$ alloys (Figures 8 (b), (c), (d)) qualitatively match the diffraction pattern of the $Sn_2Bi_2Te_5$ compound (Figure 8 (a)). The diffraction lines shift slightly relative to $Sn_2Bi_2Te_5$ due to changes in lattice parameters caused by solid solution formation.

The diffraction patterns of 20 and 40 mol% $Sn_2Bi_2Te_5$ samples (Figures 8 (f), (e)) indicate that these samples are nonhomogeneous. Analysis showed that they are two-phase and three-phase, respectively.

Figure 9 displays SEM results for selected samples of the $Sn_2Bi_2Te_5$-$Pb_2Bi_2Te_5$ section, corresponding to points 1, 2, and 3 in Figure 6. These observations confirm the diagram in Figure 6.

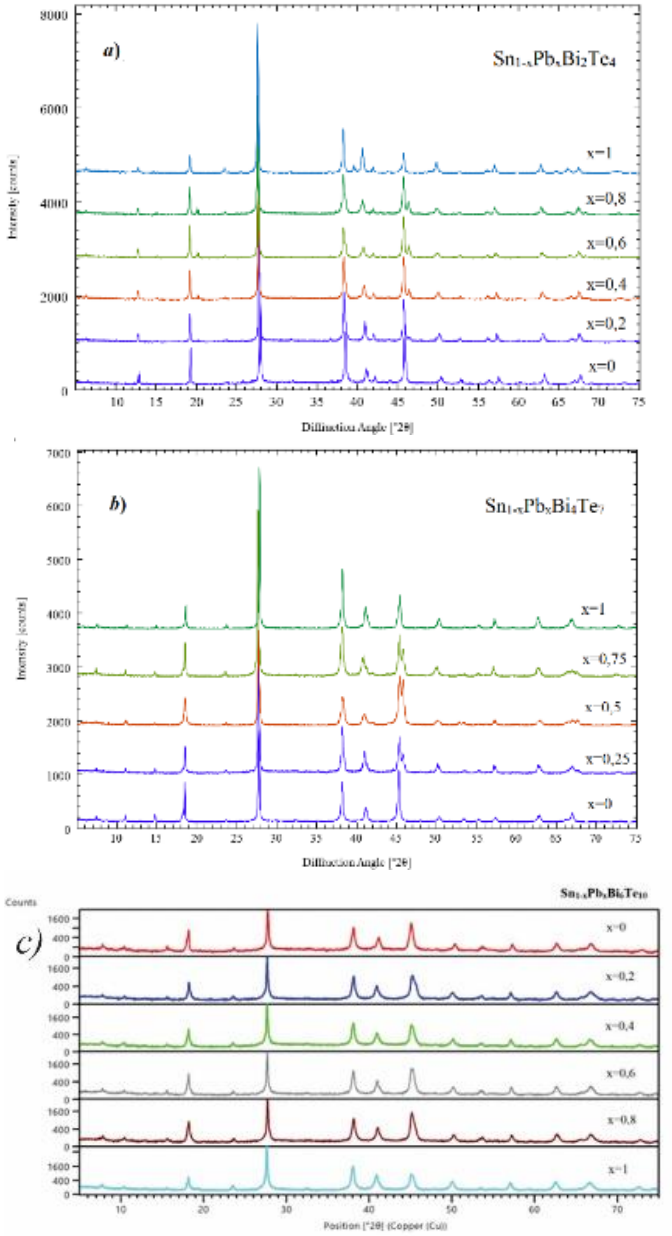

Figure 7. PXRD results for $SnBi_2Te_4$-$PbBi_2Te_4$ (a)), $SnBi_4Te_7$-$PbBi_4Te_7$ (b)), $SnBi_6Te_{10}$-$PbBi_6Te_{10}$ (c)) sections

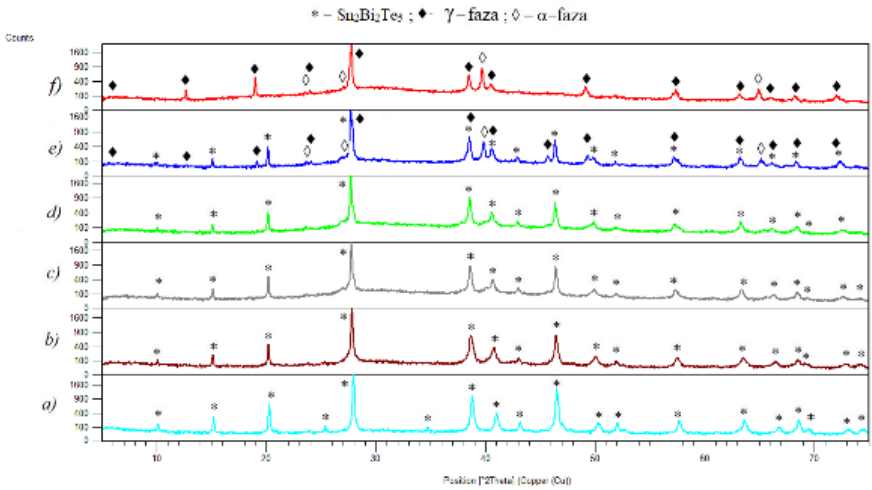

Figure 8. PXRD results for $Sn_2Bi_2Te_5$-"$Pb_2Bi_2Te_5$" section

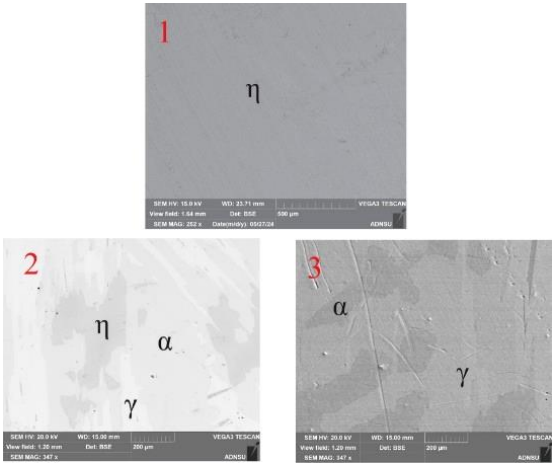

Figure 9. SEM images of samples 1, 2 and 3 (see figure 6).

Figure 10 projects the liquidus surface onto the compositional triangle. The liquidus comprises six primary crystallization fields. As shown in Figure 10, the homogeneity region of the continuous solid solutions formed in the SnTe-PbTe system penetrates deeply into the

compositional triangle, creating a broad homogeneous band (α-phase) along this subsystem. The primary crystallization field of this phase extends further into the compositional triangle, reaching approximately 62-63 mol% Bi_2Te_3 and occupying 85% of its total area. Solid solutions based on Bi_2Te_3 (β-phase) crystallize first from the melt in the region adjacent to the Bi_2Te_3 apex (region 6).

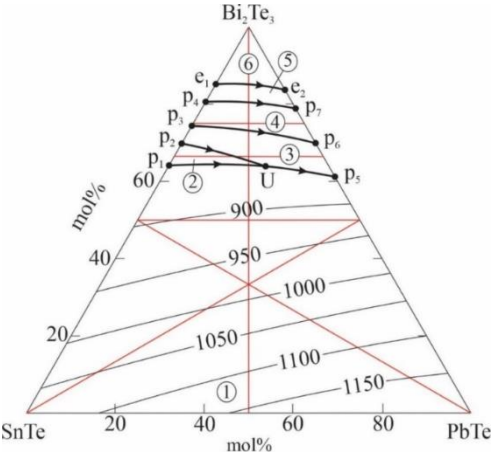

Figure 10. Projection of the liquidus surface of the SnTe-PbTe-Bi_2Te_3 system.

Among ternary compounds, the liquidus surfaces of the continuous γ-, δ-, and ε-solid solution series form narrow bands between the SnTe-Bi_2Te_3 and PbTe-Bi_2Te_3 edges (regions 3-5). These liquidus surfaces are bounded by the following monovariant equilibrium curves:

$L+\gamma \leftrightarrow \delta$ (p_3p_6 curve, 863-856 K)
$L+\delta \leftrightarrow \varepsilon$ (p_4p_7 curve, 859-851 K)
$L \leftrightarrow \beta+\varepsilon$ (e_1e_2 curve, 850-848 K)

The incongruently melting (870 K) $Sn_2Bi_2Te_5$ compound formed in the SnTe-Bi_2Te_3 system generates a wide solid solution region (η-phase) in the examined system. The primary crystallization field of this phase corresponds to region 2 on the liquidus surface. Monovariant peritectic equilibria are observed along the following curves bounding this surface:

$$L+\alpha \leftrightarrow \eta \ (p_1U \text{ curve, } 870\text{-}865 \text{ K})$$
$$L+\eta \leftrightarrow \gamma \ (p_2U \text{ curve, } 867\text{-}865 \text{ K})$$

These curves converge at the U-point, creating a nonvariant transition equilibrium:

$$L+\eta \leftrightarrow \alpha+\gamma \ (U\text{- point, } 865 \text{ K})$$

From the U-point, crystallization proceeds via the monovariant peritectic reaction:

$$L+\alpha \leftrightarrow \gamma \ (Up_5 \text{ point, } 865\text{-}862 \text{ K})$$

It is noteworthy that all these monovariant equilibria (reactions) occur over narrow temperature ranges. This is attributed to the close melting (decomposition) temperatures of isostructural ternary compounds forming continuous solid solutions. Typically, such melting involves an extremum (usually a minimum) on the liquidus (or peritectic) curves, but this is not observed here. The melting of solid solutions (or their decomposition via peritectic reactions) occurs over a very narrow temperature range between the respective melting (peritectic) points of the initial ternary compounds.

The lack of extreme deviations suggests that Sn→Pb substitutions in similar crystal lattices ($SnBi_2Te_4$-$PbBi_2Te_4$, $SnBi_4Te_7$-$PbBi_4Te_7$, $SnBi_6Te_{10}$-$PbBi_6Te_{10}$) involve relatively few atoms, causing negligible stress or deformation. Consequently, the solid solutions formed can be considered quasi-ideal. A review of extensive literature data indicates that phase diagrams of systems with minimal deviations from ideality in both liquid and solid solutions rarely display extremum.

The constructed liquidus surface projection reveals that γ-, δ-, ε-, and η-solid solutions crystallize initially from nonstoichiometric liquid phases over narrow compositional ranges (regions $p_3p_2Up_5p_6$, $p_4p_3p_6p_7$, $p_4e_1e_2p_7$ and p_1p_2U in Figure 6). The difficulty in obtaining homogeneous single crystals of these phases stems from this. For growing single crystals, the "melt-solution" composition must be precisely selected.

Some isopleth sections of the phase diagram. Figure 11 provides the polythermal section for $SnBi_2Te_4$-$PbBi_2Te_4$. As shown in Figure 7(a), continuous substitution solid solutions form along this section. This is reflected in the T-x diagram provided in Figure 11. The phase diagram indicates that the polythermal section lies entirely in the primary crystallization field of the α-solid solutions. Thus, the α-phase crystallizes first

from the liquid solution, leading to the formation of the L+α biphasic field. Below the liquidus, crystallization becomes complex. A comparison with Figure 6 shows that crystallization proceeds via the peritectic reaction (4) in the 0-60 mol% $PbBi_2Te_4$ composition interval and via reaction (7) in the >60 mol% $PbBi_2Te_4$ region. These monovariant reactions result in the formation of L+α+η and L+α+γ triphasic fields. Subsequent crystallization processes occur over a narrow temperature range (870-862 K), and the thermal effects characterizing them could not be detected through DTA curves. Even slow heating (3-5 °C/min) of very small samples (0.1 g) yielded DTA curves with a broad peak.

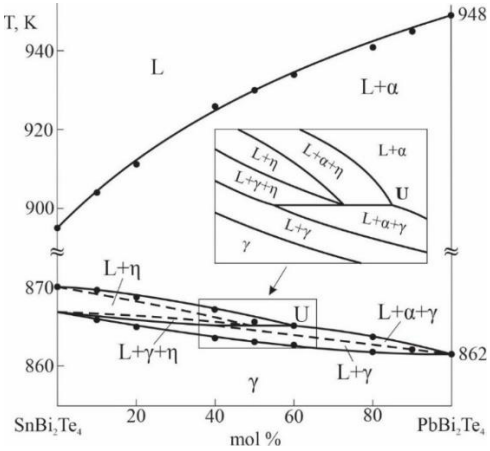

Figure 11. Isopleth section $SnBi_2Te_4$-$PbBi_2Te_4$ of the phase diagram

This chapter also presents polythermal sections for $SnBi_2Te_4$-$PbBi_2Te_4$, $SnBi_4Te_7$-$PbBi_4Te_7$, $SnBi_6Te_{10}$-$PbBi_6Te_{10}$, and perpendicular lines from the compositional triangle's vertices to opposite edges: SnTe-$PbBi_2Te_4$, PbTe-$SnBi_2Te_4$, Bi_2Te_3-$Sn_{0,5}Pb_{0,5}Te$.

The fourth chapter presents the results of the 3D modeling of phase diagrams for the SnTe-PbTe-Bi_2Te_3 and PbTe-Bi_2Te_3-Sb_2Te_3 systems. Initially, the thermodynamic foundations of phase equilibria and the basic principles of 3D modeling are explained at the beginning of the chapter. Subsequently, using an analytical method, the liquidus and solidus surfaces of the SnTe-PbTe-Bi_2Te_3 and PbTe-Bi_2Te_3-Sb_2Te_3 systems were modeled in 3D (34861 characters).

Multicomponent 3D Modeling of Phase Diagrams for PbTe-Bi_2Te_3-Sb_2Te_3 and SnTe-PbTe-Bi_2Te_3 systems. The molar Gibbs energy of liquid and solid solutions in ternary chalcogenide systems can be calculated based on the corresponding thermodynamic functions of their boundary binary systems:

$$\Delta\overline{G}_1^{\text{iz.}} = \frac{x_2}{x_2+x_3}\left[\Delta\overline{G}_{1(12)}^{\text{iz.}}\right]_{x_1} + \frac{x_3}{x_2+x_3}\left[\Delta\overline{G}_{1(13)}^{\text{iz.}}\right]_{x_1} + a_1 x_1 x_2 x_3 \quad (1)$$

$$\Delta\overline{G}_2^{\text{iz.}} = \frac{x_1}{x_1+x_3}\left[\Delta\overline{G}_{2(12)}^{\text{iz.}}\right]_{x_2} + \frac{x_3}{x_1+x_3}\left[\Delta\overline{G}_{2(13)}^{\text{iz.}}\right]_{x_2} + a_2 x_1 x_2 x_3 \quad (2)$$

$$\Delta\overline{G}_3^{\text{iz.}} = \frac{x_2}{x_2+x_1}\left[\Delta\overline{G}_{3(12)}^{\text{iz.}}\right]_{x_3} + \frac{x_1}{x_2+x_1}\left[\Delta\overline{G}_{3(13)}^{\text{iz.}}\right]_{x_3} + a_3 x_1 x_2 x_3 \quad (3)$$

In the equations above, is the partial excess Gibbs energy of the component in the boundary system. The excess partial molar thermodynamic functions of boundary systems are added based on the composition. The constant is calculated based on a few experimental parameters of the system. The thermodynamic functions of the boundary binary systems, i.e., systems 1-2, 1-3, and 2-3, can be used in the equations for the ternary system:

$$\Delta\overline{G}^{\text{iz.}} = \frac{x_2}{x_2+x_3}\left[\Delta\overline{G}_{1(12)}^{\text{iz.}}\right]_{x_1} + \frac{x_3}{x_2+x_3}\left[\Delta\overline{G}_{1(13)}^{\text{iz.}}\right]_{x_1} -$$
$$-\left(1-x_1\right)^2\left[\Delta\overline{G}_{1(23)}^{\text{iz.}}\right]x_2/x_3 + a_1 x_1 x_2 x_3 \quad (4)$$

Using the thermodynamic functions of binary systems in equations (1-4), the crystallization curves of components can be used to calculate the partial excess Gibbs energy of the common component (component 3) in systems 1-3 and 2-3:

$$\Delta\overline{G}_3^{\text{iz.,m}} = T\left(\Delta S_3^{\text{ər.}} - 19{,}144\lg x_3\right) - \Delta H_3^{\text{ər.}} \quad (5)$$

Substituting these thermodynamic functions into equation (5), we derive equations to calculate the crystallization temperatures of all components in the ternary system 1-2-3:

$$T = \frac{\Delta H_1^{\text{ər.}} + \frac{x_2}{x_2 + x_3}\left[\Delta \overline{G}_{1(12)}^{\text{iz.}}\right]_{x_1} + \frac{x_3}{x_2 + x_3}\left[\Delta \overline{G}_{1(13)}^{\text{iz.}}\right]_{x_1} + a_1 x_1 x_2 x_3}{\Delta S_1^{\text{ər.}} - 8.31 \ln x_1} \quad (6)$$

$$T = \frac{\Delta H_2^{\text{ər.}} + \frac{x_1}{x_1 + x_3}\left[\Delta \overline{G}_{2(12)}^{\text{iz.}}\right]_{x_2} + \frac{x_3}{x_1 + x_3}\left[\Delta \overline{G}_{3(13)}^{\text{iz.}}\right]_{x_2} + a_2 x_1 x_2 x_3}{\Delta S_2^{\text{ər.}} - 8.31 \ln x_2} \quad (7)$$

$$T = \frac{\Delta H_3^{\text{ər.}} + \frac{x_2}{x_1 + x_2}\left[\Delta \overline{G}_{3(23)}^{\text{iz.}}\right]_{x_3} + \frac{x_1}{x_2 + x_1}\left[\Delta \overline{G}_{3(13)}^{\text{iz.}}\right]_{x_3} + a_3 x_1 x_2 x_3}{\Delta S_3^{\text{ər.}} - 8.31 \ln x_3} \quad (8)$$

Equations (6-8) rely on the molar melting enthalpy ($\Delta H_i^{\text{ər}}$) and entropy ($\Delta S_i^{\text{ər}}$) of the component. If the experimental values for the melting entropy and enthalpy of a compound are unavailable, they are calculated using equations (9-11), based on the molar formation enthalpy ($\Delta H_{i,T}^0$) and entropy ($\Delta S_{i,T}^0$) of the primary components of the compound:

$$T = \frac{\Delta H_1^0 + \frac{x_2}{x_2 + x_3}\left[\Delta \overline{G}_{1(12)}^{\text{iz.}}\right]_{x_1} + \frac{x_3}{x_2 + x_3}\left[\Delta \overline{G}_{1(13)}^{\text{iz.}}\right]_{x_1} + a_1 x_1 x_2 x_3}{\Delta S_1^0 - 8.31 \ln x_1} \quad (9)$$

$$T = \frac{\Delta H_2^0 + \frac{x_1}{x_1 + x_3}\left[\Delta \overline{G}_{2(12)}^{\text{iz.}}\right]_{x_2} + \frac{x_3}{x_1 + x_3}\left[\Delta \overline{G}_{3(13)}^{\text{iz.}}\right]_{x_2} + a_2 x_1 x_2 x_3}{\Delta S_2^0 - 8.31 \ln x_2} \quad (10)$$

$$T = \frac{\Delta H_3^0 + \frac{x_2}{x_1 + x_2}\left[\Delta \overline{G}_{3(23)}^{\text{iz.}}\right]_{x_3} + \frac{x_1}{x_2 + x_1}\left[\Delta \overline{G}_{3(13)}^{\text{iz.}}\right]_{x_3} + a_3 x_1 x_2 x_3}{\Delta S_3^0 - 8.31 \ln x_3} \quad (11)$$

Equations (6-11) describe the primary crystallization surface (liquidus surface) related to the bivariant equilibrium of a component or a ternary compound in the system. The intersection of two surfaces represents the crystallization process of two substances. These lines correspond to the coordinates of monovariant equilibria. The intersection of liquidus curves determines the nonvariant equilibrium point, defining the composition and temperature of the ternary eutectic.

Table 2

Analytical relations of the phases of the Sb_2Te_3-PbTe-Bi_2Te_3 system

Phase number in Figure 12	T,K=f(x,y); x=x(PbTe): y=x(Bi_2Te_3)/[x(Sb_2Te_3)+ x(Bi_2Te_3)]; x_i- PbTe, Bi_2Te_3, Sb_2Te_3 are the molar concentrations of the compounds
1	(1197-351*(1-x)-276.7*(1-x)^2-26.8*(1-x)^3)*y+ (653+539*x+5.8*x^2)*(1-y)+70*y*(1-y)*(1-x) x=0÷0.625, y=0÷1
2	(-268+1465*x+9728*(1-x)^2-91304*(1-x)^3)*y +(58828+113775*x-53750*x^2)*(1-y) x=0.96÷1, y=0÷1; (446+4325*x-10545*x^2)*(1-y)+ (443,5+2065*x)*y, x=0.832÷0.954, y=0÷1
5	694.5+593.7*(1-x)-518.5*(1-x)^2)*y+(765+250*x) *(1-y) +70*y*(1-y)*(1-x) x=0.625÷0.71, y=0÷0.95
6	(776,4+264,5*x-215,4*x^2)*(1-y)+(596,6+ 677,5* x-437,5*x^2)*y, x=0.695÷0.875, y=0÷1
7	(546+592*x-280*x^2)*(1-y)+(731+130*x)*y, x=0.81÷0.875, y=0÷1
9	(629,6+421,9*(1-x)-190,5*(1-x)^2)*y+(895-46*x-180*x^2)*(1-y)+70*y*(1-y)*(1-x); y=0÷1
11	(-13642+34100*x-20000*x^2). x=0.9÷0.97, y=0÷1
12,13,14	12550+26300*x; 9542-26300*x; -5975+26300*x

After thermodynamic calculations of high-melting-temperature regions of the phase diagrams, the system was modeled using the analytical option of the OriginLab software. An analytical 3D modeling method, successfully tested in previous works, was used for visualizing the liquidus surfaces.

The analytical dependencies for the 3D modeling of phases in the PbTe-Sb_2Te_3-Bi_2Te_3 system are provided in Table 2.

Fragments of the phase diagram for the PbTe-Bi_2Te_3-Sb_2Te_3 system are visualized in Figure 12 using equations in Table 2.

The analytical dependencies for the 3D modeling of phases in the SnTe-PbTe-Bi_2Te_3 system are provided in Table 3. These equations allow for the visualization of individual phase surfaces as well as all phases in a single graph (Figure13).

Table 3

Analytical relations of the phases of the SnTe-PbTe-Bi_2Te_3 system

Phase number in Figure 13	T,K=f(x,y);x=x(Bi_2Te_3),y=x(SnTe/[x(SnTe)+x(PbTe)]; x_i=SnTe, PbTe, Bi_2Te_3 mole fraction of compounds
1	-(1197-351*x-276,7*x^2-26,8*x^3)*(1-y)+(1079-211,33*x-189,7*x^2-102,1*x^3)*y+16*y*(1-y); x=0÷0.625, y=0÷1
2	(1197-1465,3*x+9728*x^2-91304*x^3)*(1-y)+(1079-1923,1*x+5841,7*x^2-6624,48*x^3)*y-48*y*(1-y), x=0÷0.158, y=0÷1; (446+4325*x-10545*x^2)*(1-y)+(443,5+2065*x)*y, x=0.046÷0.168, y=0÷1;
5	(760+374*x-308*x^2)*y+(694,5+593,7*x-518,5*x^2)*(1-y), x=0.625÷0.71, y=0÷0.95;
6	(776,4+264,5*x-215,4*x^2)*(1-y)+(596,6+677,5*x-437,5*x^2)*y, x=0.695÷0.875, y=0÷1;
7	(546+592*x-280*x^2)*(1-y)+(731+130*x)*y, x=0.81÷0.875, y=0÷1
9	(-12550+26300*x), x=0.5÷0.51, y=0÷1
10	(-16942+26300*x), x=0.667÷0.677, y=0÷0.8;
11	(-19125+26300*x), x=0.75÷0.759, y=0÷1
12	(-13642+34100*x-20000*x^2). x=0.9÷0.97, y=0÷1

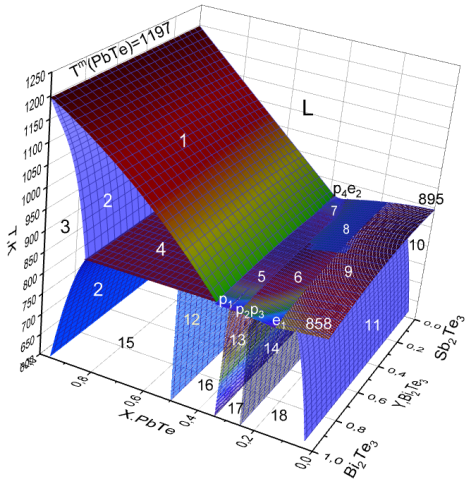

Figure 12. 3D view of the phase diagram of the PbTe-Bi_2Te_3-Sb_2Te_3 system from the PbTe-Bi_2Te_3 system side.

1- The liquidus surface of solid solutions based on α(PbTe); 2- The solidus surface of solid solutions based on α(PbTe); 3- The field of solid solutions based on α(PbTe); 4- The plane where the peritectic compound $PbBi_2Te_4$ forms; 5- The liquidus surface of the peritectic compound $PbBi_2Te_4$; 6- The liquidus surface of the peritectic compounds $PbBi_4Te_7$ and $PbBi_6Te_{10}$; 7- The liquidus surface of the peritectic compound $Pb_2Sb_6Te_{11}$; 8- The liquidus surface of solid solutions based on β-Bi_2Te_3; 9- The liquidus surface of solid solutions based on β-Bi_2Te_3 and β-Sb_2Te_3; 10- The field of solid solutions based on β-Bi_2Te_3 and β-Sb_2Te_3; 11- The solidus surface of solid solutions based on β-Bi_2Te_3 and β-Sb_2Te_3; 12-14: Perpendicular planes to the peritectic transformation planes of the phases $PbBi_2Te_4$, $PbBi_4Te_7$, $PbBi_6Te_{10}$; 15- The heterogeneous field of solid solutions based on α(PbTe)+ $PbBi_2Te_4$; 16- The heterogeneous field $PbBi_2Te_4$ + $PbBi_4Te_7$; 17- The heterogeneous field $PbBi_4Te_7$ + $PbBi_6Te_{10}$; 18- The heterogeneous field of solid solutions based on β-Bi_2Te_3 and β-Sb_2Te_3+ $PbBi_6Te_{10}$.

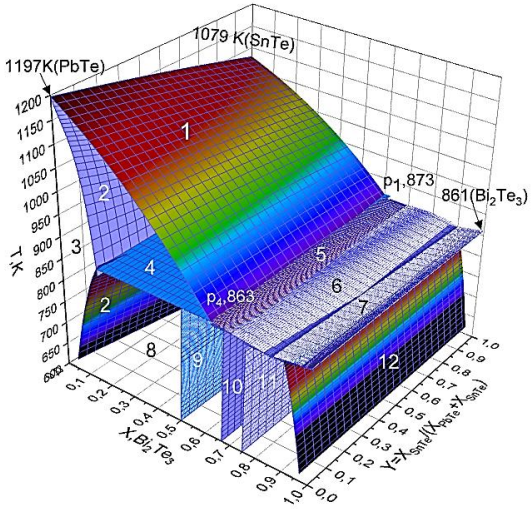

Figure 13. 3D view of the phase diagram of the SnTe-PbTe-Bi_2Te_3 system from the PbTe-Bi_2Te_3 system side.

1- The liquidus surface of solid solutions based on α (PbTe) and α (SnTe); 2- The solidus surface of solid solutions based on α(PbTe)

and α (SnTe); 3- The field of solid solutions based on α (PbTe) and α (SnTe); 4- The plane where the peritectic compounds $PbBi_2Te_4$ və $SnBi_2Te_4$ form; 5- The crystallization surface for peritectic compounds across the $p_1p_2p_4p_5$ region (see projection figure); 6- The crystallization surface for peritectic compounds across the $p_2p_5p_4p_6e_1e_2$ region; 7- The liquidus surface of solid solutions based on β-Bi_2Te_3; 8- The heterogeneous mixture of $PbBi_2Te_4$, $SnBi_2Te_4$ compounds, and solid solutions based on α(PbTe), α(SnTe); 9-11: Perpendicular planes to the peritectic transformation planes of the phases $Pb(Sn)Bi_2Te_4$, $Pb(Sn)Bi_4Te_7$, Pb(Sn); 12- The solidus surface of solid solutions based on β-Bi_2Te_3.

Thus, the 3D modeling and thermodynamic analysis of the phase diagram of both quasi-ternary systems under consideration agree well with the experimental results and show that complex systems consisting of ternary compounds, which are structural analogues of lead-bismuth tellurides, are characterized by the formation of a continuous solid solution domain that is thermodynamically stable. The thermodynamic analysis also shows that the liquid and solid solutions formed in these systems can be considered as associated regular solutions.

RESULTS

1. The nature of the physicochemical interactions of the corresponding quaternary systems PbTe-Bi_2Te_3-Sb_2Te_3 and SnTe-PbTe-Bi_2Te_3 in concentration planes was determined using DTA, DSC, XRD, and SEM methods. In both concentration triangles, the primary crystallization areas of phases and the types of nonvariant and monovariant processes reflecting phase equilibria were identified. It was shown that both concentration planes are independent quasi-ternary systems characterized by the formation of wide solid solution regions based on ternary and binary compounds with topological insulator properties [1, 8, 9, 13].
2. The liquidus surface of the PbTe-Bi_2Te_3-Sb_2Te_3 system consists of six areas representing the primary crystallization of solid solutions based on binary compounds and the ternary compounds $PbBi_2Te_4$, $PbBi_4Te_7$ and $PbBi_6Te_{10}$. These surfaces are bounded by a series of

monovariant peritectic and eutectic equilibrium curves and nonvariant peritectic, transition, and eutectic equilibrium points. Broad solid solution regions with Bi→Sb substitution were discovered based on the ternary compounds $PbBi_2Te_4$, $PbBi_4Te_7$, and $PbBi_6Te_{10}$. It was also shown that the continuous solid solution series present in the Bi_2Te_3-Sb_2Te_3 boundary system penetrates the concentration triangle, forming a homogeneity band approximately 3–8 mol% wide [1, 2, 3, 9, 10].

3. In the SnTe-PbTe-Bi_2Te_3 quasi-ternary system, the liquidus also consists of six primary crystallization areas. Continuous solid solution series were identified along the sections $SnBi_2Te_4$–$PbBi_2Te_4$, $SnBi_4Te_7$–$PbBi_4Te_7$, and $SnBi_6Te_{10}$–$PbBi_6Te_{10}$, along with broad homogeneity regions based on Bi_2Te_3, $Sn_2Bi_2Te_5$, and $Sn_3Bi_2Te_6$ compounds. It was shown that the solid solutions of the SnTe-PbTe boundary system penetrate up to 10 mol% into the ternary system. A characteristic feature of the system is that most of the monovariant equilibrium points on the SnTe-Bi_2Te_3 and PbTe-Bi_2Te_3 lateral systems are connected by monovariant equilibrium curves. This is associated with the existence of the above-mentioned continuous solid solution series [6, 7, 8, 13].
4. It was established that, in both quasi-ternary systems, the primary crystallization of variable-composition phases based on ternary compounds, as well as the nonvariant and monovariant equilibria, cover very small temperature intervals and concentration regions in the general T-x-y diagrams of these systems. This is related to the layered (including mixed-layered) structures of these phases, which decompose through a series of successive peritectic reactions upon melting, making it challenging to obtain ions in a homogeneous state [1, 8, 9, 13].
5. Various solid solutions with Sb→Bi and Sn→Pb substitution discovered in the studied systems were synthesized and identified individually. It was determined that they are Van der Waals phases with tetradymite-like structures and are potential topological insulator materials. The lattice parameters of the solid solutions were calculated, and it was shown that their dependency on composition satisfies Vegard's law [1, 8, 9, 13].

6. Based on the thermodynamic criteria of phase equilibria and the principles of the fuzzy logic approach, the liquidus and solidus surfaces (curves) of solid solutions based on PbTe, SnTe, Bi_2Te_3, Sb_2Te_3, $PbBi_2Te_4$, $PbBi_4Te_7$ and $PbBi_6Te_{10}$ in the PbTe-Bi_2Te_3-Sb_2Te_3 və SnTe-PbTe-Bi_2Te_3 quasi-ternary systems and their quasi-binary boundary systems were refined. The effectiveness of the physicochemical model based on the fuzzy logic approach for defining the boundaries of solid solutions was demonstrated [4, 5, 11, 12, 14, 15].
7. Analytical expressions reflecting the temperature and composition dependencies of the crystallization of solid solutions based on all binary and ternary compounds in the T-x-y diagrams of the PbTe-Bi_2Te_3-Sb_2Te_3 and SnTe-PbTe-Bi_2Te_3 systems, including phases formed via peritectic reactions, were obtained. Using these expressions, Multi 3D models of liquidus and solidus surfaces were developed and graphically visualized in volumetric phase diagrams [4, 5, 11, 12, 14, 15].

The main results of the dissertation were published in the following scientific works:

1. Aghazade, A.I. Phase equilibria of the $PbBi_2Te_4$ -$PbSb_2Te_4$ section of the PbTe - Bi_2Te_3 -Sb_2Te_3 system and some properties of the solid solutions // Azerbaijan Chemical Journal, -2020, №4, -p.53-59.
2. Aghazade, A.I., Orujlu, E.N., Gasymov, V.A., Babanly, M.B. Solid-phase equilibria in the PbTe-Bi_2Te_3-Sb_2Te_3 system // 9th Rostocker International Conference: "Thermophysical Properties for Technical Thermodynamics", - Rostock, - Germany, - 2020, -p.55.
3. Aghazade, A.I., Oruclu, E.N., Babanlı, M.B. PbTe-Bi_2Te_3–Sb_2Te_3 sistemində $PbBi_4Te_7$ əsasında bərk məhlullar // "Müasir təbiət və iqtisad elmlərinin aktual problemləri" beynəlxalq elmi konfrans, - Gəncə, -Azərbaycan, -2021, -p.28-31.
4. Aghazade, A.I., Mammadov, A.N., Babanly, M.B. Study and modeling of the phase diagram of the system Bi_2Te_3-SnTe-PbTe in the region of solid solutions based on SnTe, PbTe and peritectic phases $SnBi_2Te_4$, $PbBi_2Te_4$ // 10th Rostocker International Conference: "Thermophysical Properties for Technical Thermodynamics", -

Rostock, - Germany, - 2021, - p.7.
5. Aghazade, A.I., Mammadov, A.N., Babanly, M.B. Thermodynamic calculation and modeling of the phase diagram of the PbTe-Bi_2Te_3-Sb_2Te_3 // "1st International congress on natural sciences", (ICNAS)-Erzurum, - Turkey, - 2021, - p.117.
6. Aghazade, A.I., Orujlu, E.N., Babanly, M.B. Experimental investigation of solid-phase equilibria in the SnTe-PbTe-Bi_2Te_3 system // XI Международная научная конференция "Кинетика и механизм кристаллизации. Кристаллизация и материалы нового поколения", - Иваново, - Россия, -2021, -p.229-230.
7. Aghazade, A.I., Orujlu, E.N., Sultanova, S.G., Babanly, M.B. Solid solutions in the $SnBi_2Te_4$-$PbBi_2Te_4$ system // "Физико-химические процессы в конденсированных средах и на межфазных границах", -Воронеж, -2022, -p.164-165.
8. Aghazade, A.I. Phase relations and characterization of solid solutions in the $SnBi_2Te_4$-$PbBi_2Te_4$ and $SnBi_4Te_7$-$PbBi_4Te_7$ systems // Azerbaijan Chemical Journal, -2022. №3, - p.75-80.
9. Aghazade, A.I. New topological insulator phases of variable composition in the PbTe–Bi_2Te_3–Sb_2Te_3 system / A.I.Aghazade, E.N.Orujlu, S.Z. Imamaliyeva [et al.] // Properties and uses of antimony, Nova publishers, – 2022, – p.96–112.
10. Aghazade, A.I., Oruclu, E.N., Babanlı, M.B. PbTe-Bi_2Te_3-Sb_2Te_3 sisteminin likvidus səthi // "Müasir təbiət və iqtisad elmlərinin aktual problemləri" beynəlxalq elmi konfrans, -Gəncə, -Azərbaycan, - 2022, -s.12-15.
11. Aghazade, A.I., Mammadov, A.N., Babanly, M.B. Thermodynamic calculation of boundaries of solid solutions in systems PbTe–Bi_2Te_3–Sb_2Te_3 and PbTe–SnTe–Bi_2Te_3 // XXIII International Conference on Chemical Thermodynamics in Russia, - Kazan, - Russia, -2022, -p.160.
12. Aghazade, A.I. 3D modeling of phase diagram of the ternary SnTe-PbTe-Bi_2Te_3 system / A.I.Aghazade, V.I.Babanly, I.M.Gojayeva [et al.] // Azerbaijan Chemical Journal, -2023, №2, -p.62-68.
13. Aghazade, A.I. Experimental investigation of the solid phase equilibria at 300 K in the $SnBi_2Te_4$–$PbBi_2Te_4$–Bi_2Te_3 system / A.I.Aghazade, E.N.Orujlu, Z.E.Salimov [et al.] // Physics and

Chemistry of Solid State, – 2023. №3, – p. 453–459.
14. Aghazade, A.I. Multi-3D modeling of phase diagram of PbTe-Bi_2Te_3-Sb_2Te_3 system / A.I.Aghazade, S.M.Rustamova, I.M.Gojayeva [et al.] // Chemical Problems, - 2023. №4, - p.353-360.
15. Aghazade, A.I., Oruclu, E.N., Məmmədov, A.N., Babanlı, M.B. SnTe-PbTe-Bi_2Te_3 sistemində qalay və qurğuşun telluridləri əsasında bərk məhlulların kristallaşma səthlərinin təyini və analitik 3D modelləşdirilməsi // "Müasir təbiət və iqtisad elmlərinin aktual problemləri" beynəlxalq elmi konfrans, - Gəncə, - Azərbaycan, -2023, - p.18-20.

The defence will be held on _____ _____ 2025 at _____ at the meeting of the Dissertation Council ED 2.16 of Supreme Attestation Commission under President of the Republic of Azerbaijan operating at Baku State University.

Address: Academician Zahid Khalilov street, 33, Baku AZ1148, Baku State University, main building

Dissertation is accessible at the Baku State University library.

Electronic versions of the dissertation and abstract are available on the official website of the Baku State University.

Abstract was sent to the required address on ____ _____2025.

Signed for print: 14.03.2025

Paper format: 60x84$^{1/16}$

Volume: 36006

Number of hard copies: 20